

Validation of a Computational Method for the Calculation of the Flow in the Exhaust of a Low- Pressure Steam Turbine

Ulvi Fatullayev¹

¹ Duisburg, Germany

Publication Date: 2025/06/12

Abstract: This study presents the validation of a computational method for predicting flow characteristics in the exhaust of a low-pressure steam turbine, with specific focus on modeling the last stage and exhaust hood as an integrated system. Using the ANSYS CFX solver, numerical simulations were carried out on both a one-passage model and a full-geometry model, including variations in tip clearance, mesh density, and interface treatment. Experimental data from a scaled turbine model at ITSM Stuttgart were used for validation. The study investigates the influence of rotor tip clearance, mesh refinement strategies, and circumferential non-uniformities on diffuser and exhaust hood performance. Simulation results were benchmarked against measurements under different operating conditions—part load, design, and overload. After validating the computational method, it was applied to a Siemens-type single side exhaust hood to evaluate performance and identify loss mechanisms. The findings support the feasibility of the Last Stage Modeling (LSM) approach and offer optimization insights for future low-pressure steam turbine designs.

Keywords: Steam Turbine, Exhaust Hood, Diffuser, CFD, Validation, Tip Clearance, Pressure Recovery, Mesh Sensitivity.

How to Cite: Ulvi Fatullayev (2025) Validation of a Computational Method for the Calculation of the Flow in the Exhaust of a Low- Pressure Steam Turbine *International Journal of Innovative Science and Research Technology*, 10(5), 4417-4434. <https://doi.org/10.38124/ijisrt/25may2074>

I. INTRODUCTION

The use of Computational Fluid Dynamics (CFD) has become integral to the modern design and optimization of steam turbines, particularly for improving thermodynamic performance in the low-pressure section. Historically, CFD has been predominantly applied to turbine blade design. However, recent advances in computational power and modeling techniques have extended its application to off-blade areas, particularly the exhaust hood, which connects the turbine's last stage to the condenser.

The exhaust hood consists primarily of a diffuser and a collector. The diffuser decelerates the high-speed steam leaving the last stage and transforms part of its kinetic energy into static pressure—this process is known as static pressure recovery. A well-designed diffuser reduces the back pressure at the last stage, thereby increasing the turbine's enthalpy

drop and enhancing overall efficiency. The collector then guides the flow into the condenser. The performance of the diffuser and the design of the collector are closely coupled; therefore, their combined optimization is essential for minimizing energy losses.

To illustrate the functional principle of the diffuser, Figure 1.1 represents enthalpy-entropy (h-s) diagrams with and without a diffuser. In the absence of a diffuser, steam exiting the last stage retains high kinetic energy, and subsequent pressure recovery in the collector is limited, resulting in a smaller enthalpy gradient. When a diffuser is present, a portion of the kinetic energy is converted into pressure energy, raising the diffuser outlet pressure and effectively lowering the stage outlet pressure below condenser pressure. This results in a higher useful enthalpy gradient and improved turbine efficiency.

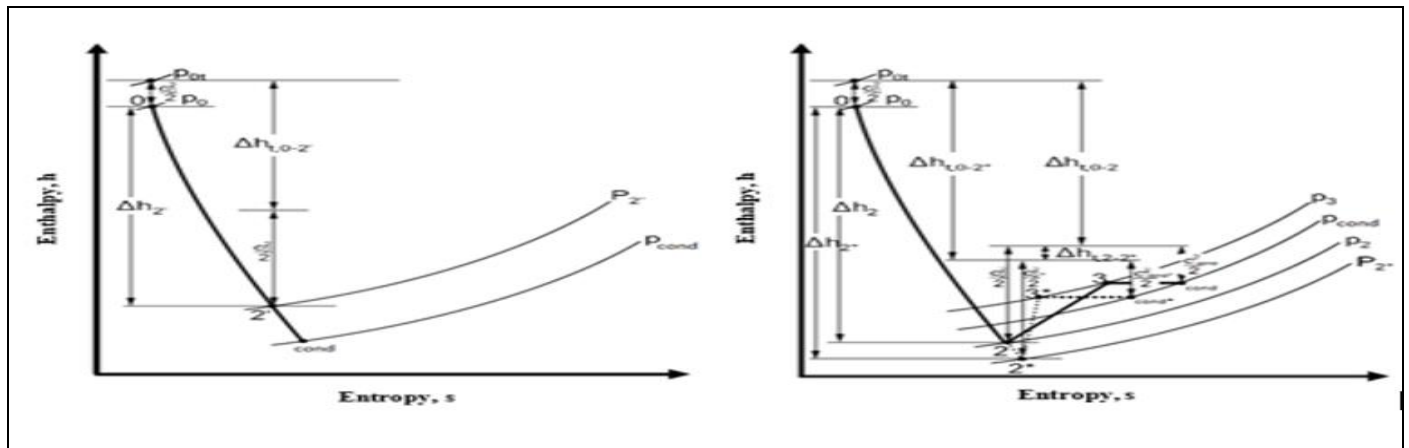


Fig 1 H-S Diagram Comparing Steam Turbine Operation without (Left) and With (Right) Diffuser [1]

Enhancing the diffuser design leads to even greater gains in static pressure recovery, as indicated by the steeper slope and reduced entropy generation in the h-s diagram. The improvements reduce energy dissipation and increase the effective enthalpy drop between the turbine inlet and condenser.

Accurate CFD modeling of these complex flow phenomena is crucial. Earlier models often excluded the last stage and approximated its effects using boundary conditions. However, with increasing computational capabilities, models now increasingly include both the last stage and the exhaust hood, providing a more realistic simulation of the flow behavior. This holistic approach, termed Last Stage Modeling (LSM), allows for the prediction of interdependencies between stage performance and exhaust behavior, particularly under off-design operating conditions.

This research aims to validate the LSM method by comparing simulation results with experimental data from a model turbine operated at the Institute for Thermal Flow Machinery (ITSM) in Stuttgart. The validation process involves mesh sensitivity studies, rotor tip clearance analysis, and interface type assessments across various operational loads. A validated model is then applied to a Siemens-type Single Side Exhaust (SSE) configuration, with the objective of evaluating performance and identifying loss mechanisms. Ultimately, the study seeks to reinforce the reliability of the LSM approach as a predictive design tool and to provide practical recommendations for future turbine optimization efforts.

II. METHODOLOGY

➤ Theoretical Background

The commercial solver ANSYS CFX-5 is utilized for numerical simulations.

The fundamental equations of CFD stem from conservation laws of mass, momentum, and energy. These are known as the Navier-Stokes equations. Due to computational constraints, the time-averaged form—Reynolds-Averaged Navier-Stokes (RANS) equations—is commonly used. For variable-density flows, Favre-averaged forms are applied.

Turbulence modelling is crucial to resolve the unknowns in the RANS equations. This study employs the $k-\epsilon$ turbulence model, a two-equation model widely used for practical engineering problems. It calculates turbulent viscosity based on turbulent kinetic energy (k) and its dissipation rate (ϵ), using transport equations derived from the gradient diffusion hypothesis.

To solve the governing equations, discretization is performed. ANSYS CFX uses the Element-based Finite Volume Method (EbFVM). The domain is subdivided into elements with nodes at their corners. Control volumes are formed around each node, and the governing equations are integrated over these control volumes using the midpoint rule for numerical integration [2].

➤ Boundary Conditions

To solve the averaged Navier-Stokes equations, appropriate boundary conditions must be specified. The boundary types used in this study include wall, inlet, outlet, and interface conditions.

Wall shear stresses are determined using scalable wall functions based on a logarithmic velocity profile approximation near the wall. For the $k-\epsilon$ turbulence model, no-slip conditions are applied, setting near-wall velocity to zero. Heat flux across smooth walls is assumed to be zero.

In this work, the stator blade, stator hub, shroud, and exhaust hood walls are modeled as stationary walls. The rotor blade and rotor hub are rotating, while the rotor shroud, and diffuser shells (when in rotating frame) are counter-rotating.

Inlet conditions are derived from streamline curvature analysis [3]. At the stator inlet, total pressure, cylindrical velocity components, and total enthalpy define the boundary. The flow is subsonic, with a turbulence intensity of 5%. The area-averaged static pressure at the outlet serves as the outlet boundary condition.

Interface boundaries are used where domains with different reference frames interact. Models used in this study comprise 3 or 4 domains depending on geometry. For example, the one-passage model includes stator, rotor,

diffuser, and collector, while the full geometry model merges the last two into an exhaust hood. The stator-rotor interface uses the stage interface, which circumferentially averages flow variables and realistically mimics time-averaged mixing losses in axial gaps [4]. The rotor-diffuser interface uses either a stage or frozen rotor interface, where the frozen rotor maintains a fixed relative position and transforms velocities between frames, neglecting transient effects. In the full model, multiple stage interfaces address circumferential non-uniformity between the rotors and exhaust hood. Rotational periodicity is applied to tangential sides in single-passage models.

To simulate tip jet flow, a rotor clearance is modeled. As rotor and clearance meshes differ in topology, a General Grid Interface (GGI) is used.

➤ *Material Properties And Key Flow Parameters*

Water vapor is the working fluid. Due to low pressure and temperature in the last stage and exhaust, the steam lies in the wet region. In this research, ideal gas properties are used predominantly; only one case uses real gas.

Typical last-stage conditions produce subcooled ideal fluid behavior, which may lead to unphysical temperature-related values. To avoid this, Denton's method [5-7] is applied to derive consistent ideal gas properties.

Table 1 Standard Adapted Ideal Gas Properties

M [kg/kmol]	κ [-]	R_{fi} [J/kg K]	c_p^* [J/kg K]	c_v^* [J/kg K]	μ 10^{-5} [Pa s]	λ [W/m K]
19.047	1.063	436.5	7365.0	6928.5	1.05	0.02

Additionally, an ideal gas with properties adapted from a real gas simulation is used:

Table 2 from Real Gas Calculations Adapted Ideal Gas Properties

M [kg/kmol]	κ [-]	R_{fi} [J/kg K]	c_p^* [J/kg K]	c_v^* [J/kg K]	μ 10^{-5} [Pa s]	λ [W/m K]
19.691	1.062	422.3	7212.0	6789.7	1.05	0.02

For real gas calculations, a homogeneous binary mixture of gas and liquid states is defined using IAPWS data. Properties like enthalpy and density are interpolated by the solver. Although droplet condensation simulations are possible, they are computationally intensive and are not applied in this study.

To evaluate the performance of the last stage and exhaust system, several key flow parameters are analyzed. These parameters are derived from averaged values of flow variables across specific cross-sections. Two averaging approaches are used: Area-averaged values are applied to static variables like pressure and temperature. Mass flow-averaged values are used for dynamic variables such as total pressure, velocity, and Mach number. The Mach number, indicating compressibility effects, is evaluated in both absolute and relative frames of reference. The axial Mach number, relevant to diffuser inlet flow characterization, is reported as a mass flow average.

For assessing diffuser and exhaust hood performance, pressure recovery coefficients and total pressure loss coefficients are calculated. These parameters indicate how effectively the flow pressure is recovered downstream and how much energy is lost due to friction, mixing, or geometric effects. Additionally, the total enthalpy drop across the last stage is used to estimate the power potential generated by the turbine. This serves as a primary performance indicator for stage efficiency.

➤ *Model Description*

Initial simulations were conducted on a one passage last stage exhaust model, consisting of a stator blade, rotor blade, and a segment of the exhaust hood located at the 6 o'clock position in the full geometry. The exhaust hood is divided into two computational domains: diffuser and collector (Figure 3).

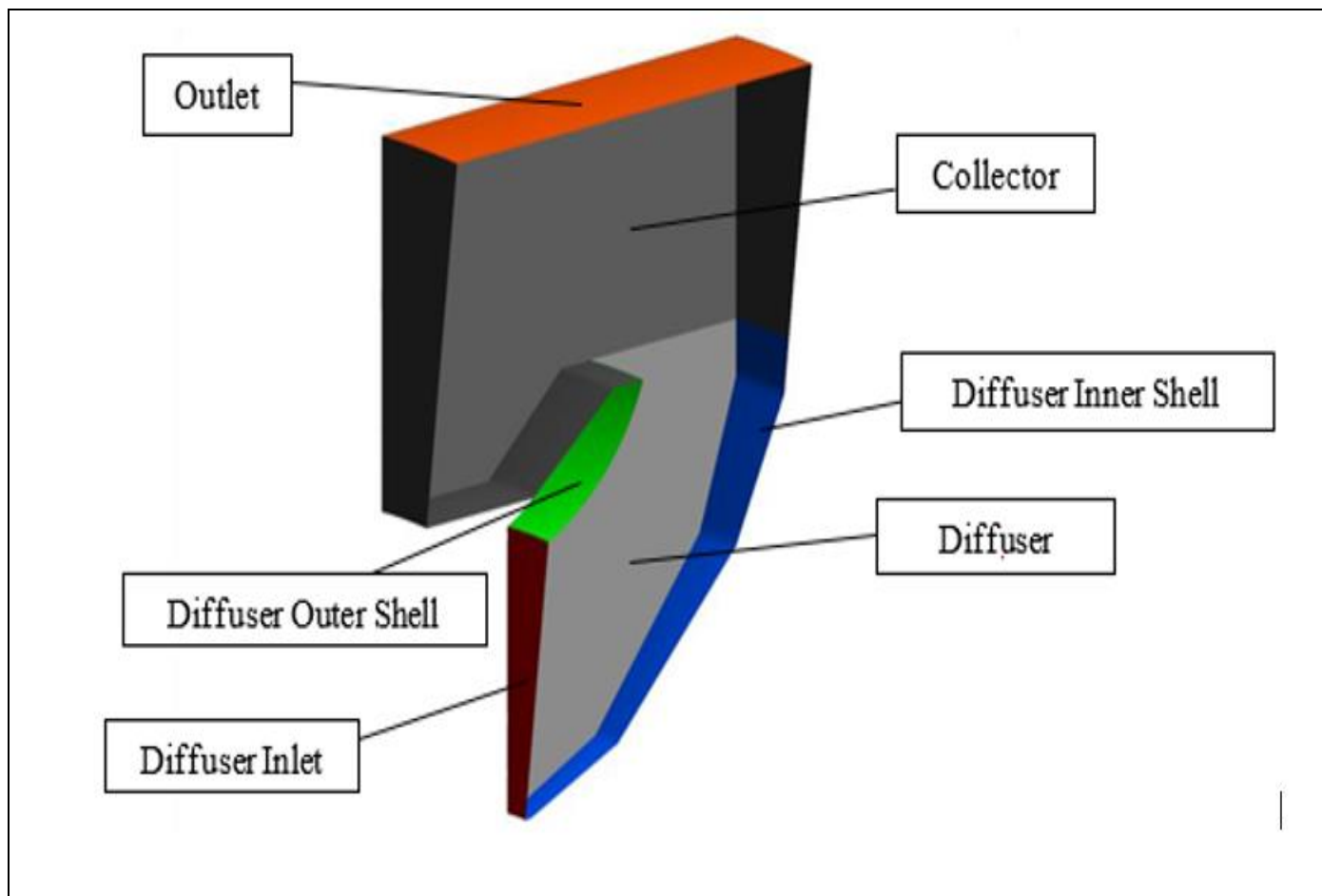


Fig 2 Exhaust Hood Slice Geometry

This model facilitates mesh sensitivity studies with reduced computational demand. Structured hexahedral meshes were generated for stator and rotor domains using Ansys CFX TurboGrid, while the diffuser employed a structured mesh and the collector an unstructured mesh via Ansys Workbench. The complete baseline mesh is shown in Figure 2.2, with 257,172 nodes and 393,603 elements.

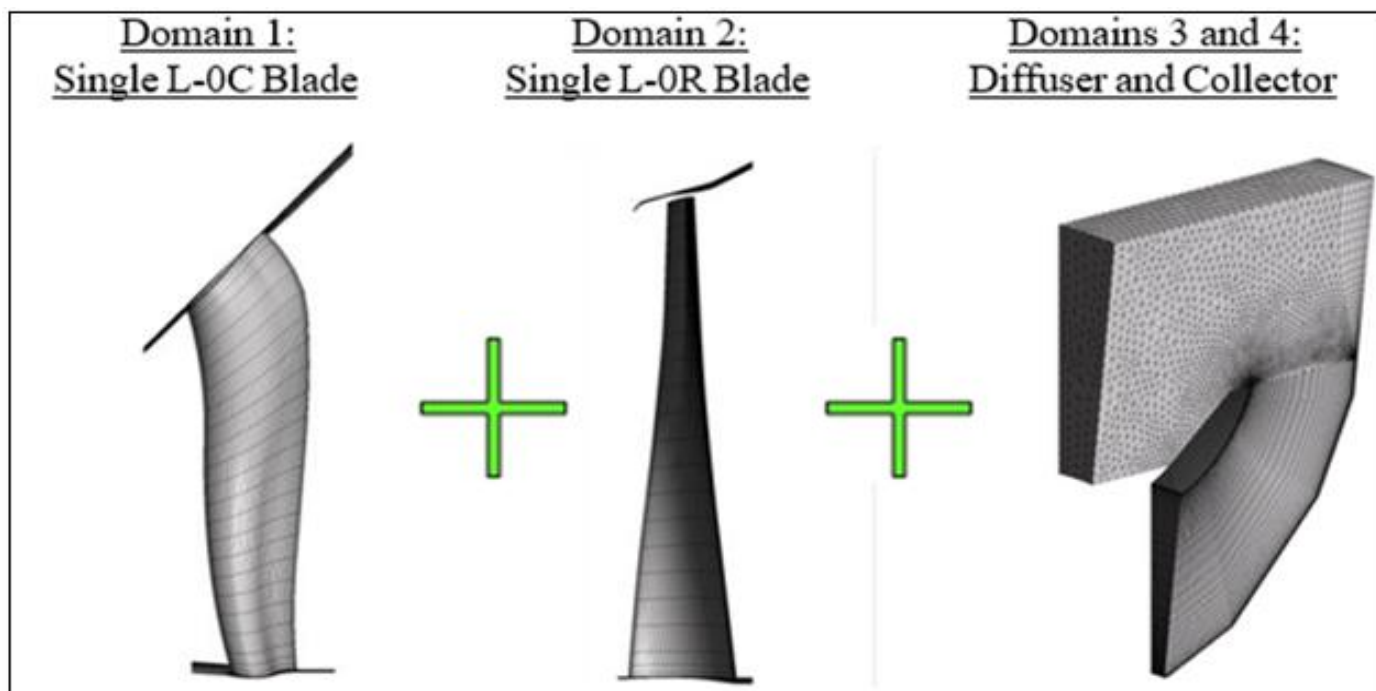


Fig 3 Meshes of the Computational Model (Baseline)

To better resolve wake effects, the diffuser domain was modeled in a rotating reference frame. The investigation included tip clearance definition, mesh sensitivity analyses, and interface configuration assessments. Due to its limitations in capturing swirl effects, this model was evaluated under design point conditions only.

To capture circumferential non-uniformity and swirl effects, simulations were also conducted using a full geometry exhaust hood model (Figure 4), consisting of a stator blade, full rotor row, and exhaust hood (Figure 5).

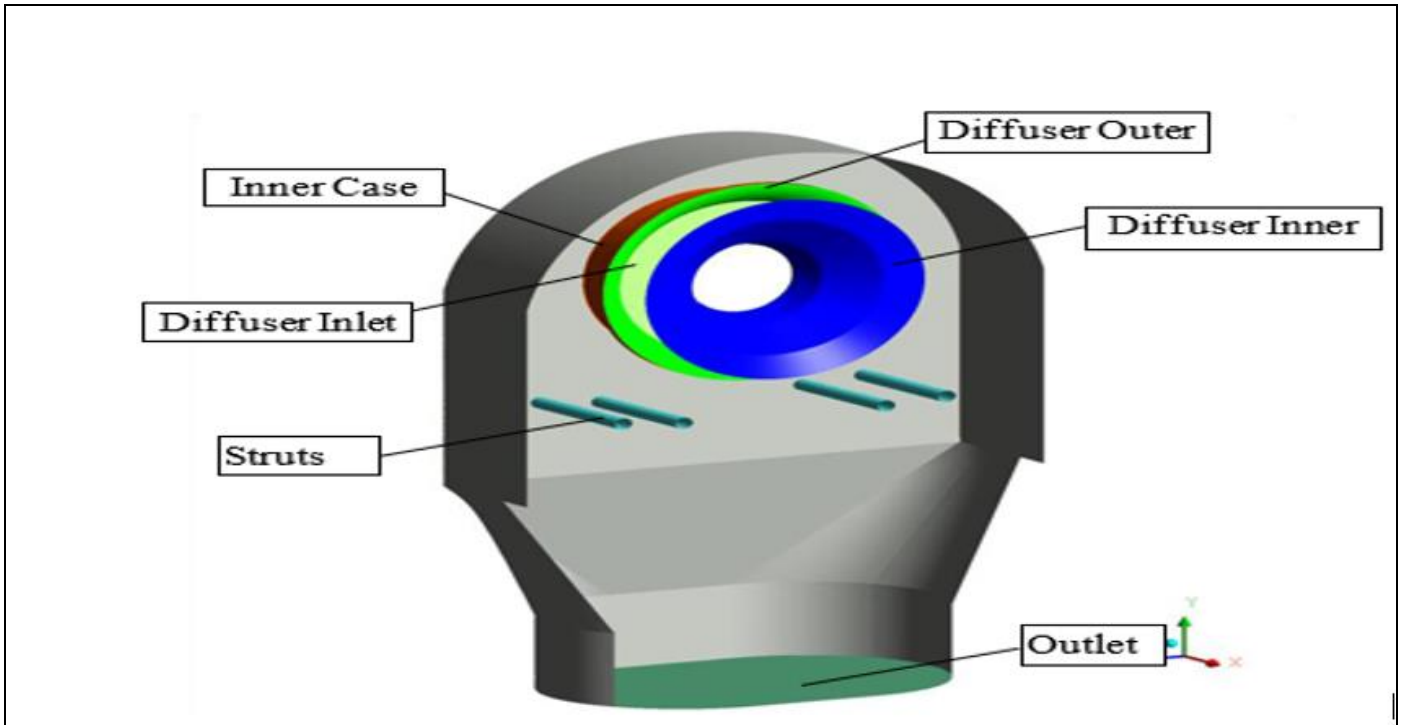


Fig 4 Exhaust Hood Geometry

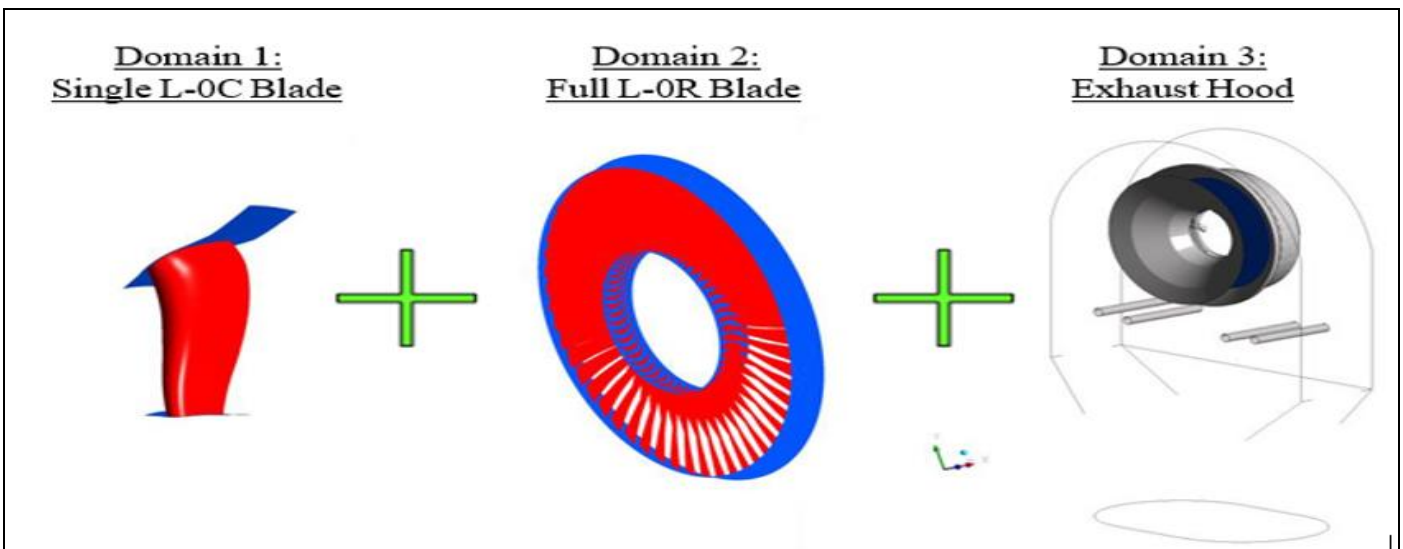


Fig 5 Computational Domains-Full Geometry

Mixing plane interface was applied between stator and rotor, and a frozen rotor interface connected rotor and diffuser. The standard k-ε turbulence model with scalable wall functions was used.

➤ *Measurements on the Model Turbine*

To validate the applied CFD methodology, experimental data from the Model Turbine at ITSM Stuttgart were used. This turbine is a three-stage scaled model (1:4) of a Siemens/KWU low-pressure steam turbine. The tip clearance is kept unscaled, while the diffuser angle is smaller than that of full-scale turbines. Figure 8 shows the locations of the measurement planes in the diffuser: Plane 32 at the inlet and Plane 40 at the outlet.

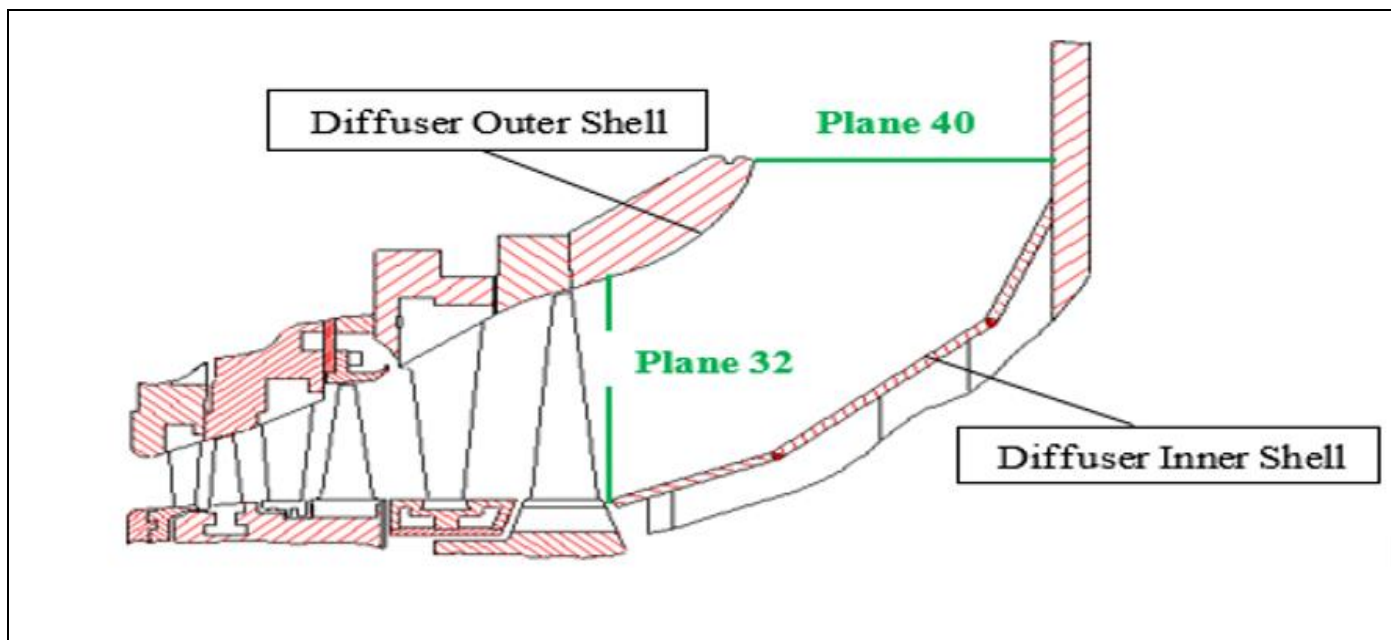


Fig 6 Location of Measuring Planes in "Model Turbine" Diffuser [8]

Spanwise static and total pressures were recorded at two circumferential positions, illustrated in Figure 6, corresponding to 1.5 stator pitches.

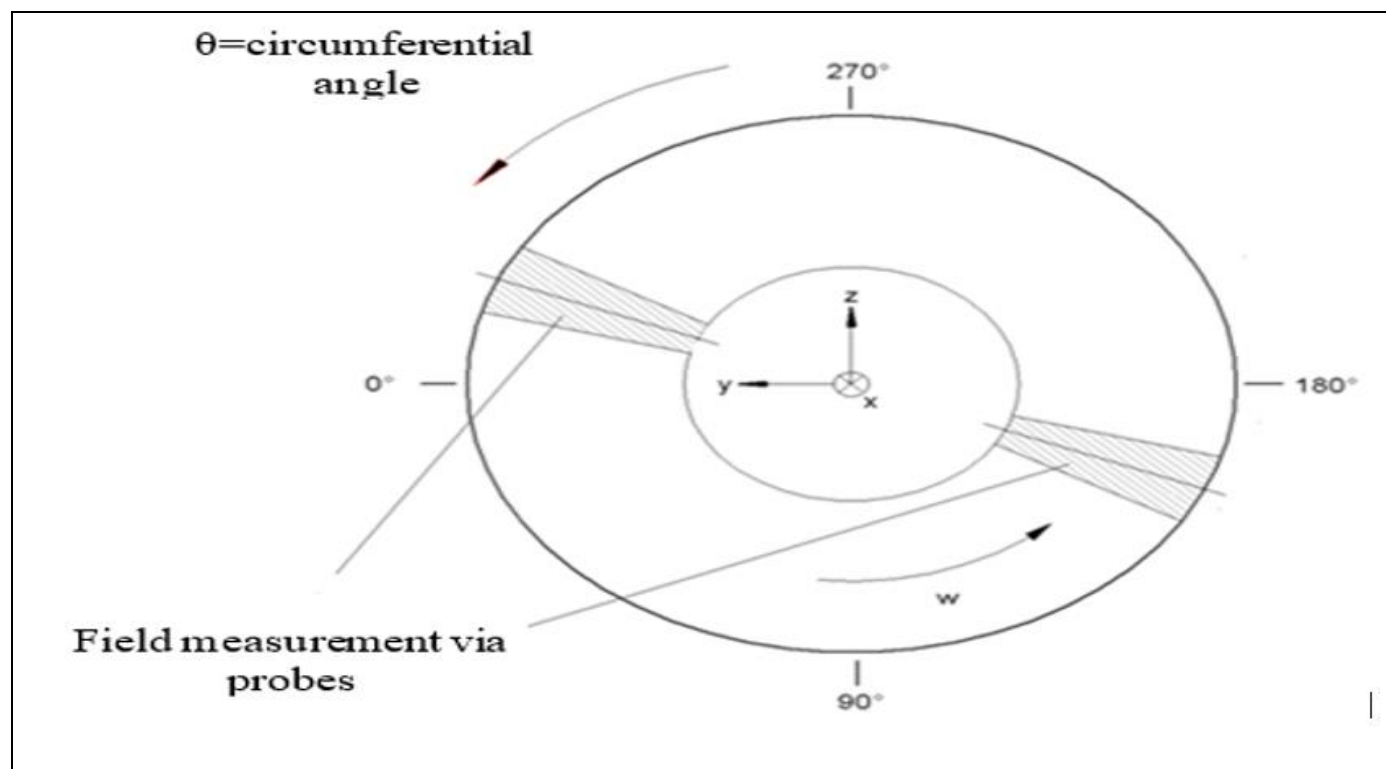


Fig 7 Circumferential Positions of the Probes at the Diffuser Inlet [9]

The diffuser inner shell (DIS) features pressure tabs at eight circumferential angles, while the diffuser outer shell

(DOS) has two tab sets with 180° offset and is designed to be rotatable.

Table 3 Operating Data

Operating Mode	Dimensionless Volume Flow Rate ϕ_{ax} [-]
Part Load	0.30
Design Load	0.42
Overload	0.61

Measurements were conducted under three operating modes—part load, design load, and overload—defined by varying flow rates, as listed in Table 3.

III. RESULTS AND DISCUSSION

To clearly present the structure of this work, the CFD analysis and simulations are categorized into two main phases, with corresponding results and discussions.

➤ Phase I – Validation On Model Turbine

The objective is to assess the accuracy and numerical robustness of the CFD method by comparing it with existing experimental data from the model turbine at ITSM Stuttgart. Measurements are available at the diffuser inlet, outlet, and along the inner and outer shells. Simulations were carried out using two exhaust configurations: the one-passage last stage exhaust model (enabling efficient mesh sensitivity studies) and the full geometry model, which accounts for circumferential flow non-uniformity. Analyses included rotor tip clearance, to identify the size that best captures the tip jet flow along the diffuser outer shell, mesh sensitivity, to find the optimal mesh-resolution-to-computational-cost ratio,

interface dependency, evaluating mixing plane vs. frozen rotor interfaces, off-design conditions, assessed only on the full geometry model due to swirl effects.

➤ Phase II – Single Side Exhaust (SSE) Calculations

The validated method is applied to a full geometry SSE turbine model. Performance curves are generated, and the influence of interface treatment and geometric modifications on diffuser and exhaust hood performance is evaluated to identify loss mechanisms and improve turbine efficiency.

➤ One Passage Last Stage Exhaust Model Calculations

• Tip Clearance Analysis

In reality, rotor tip clearance is not circumferentially uniform; however, for the simulations in this study, it is assumed to be uniform. As such, the numerical setup cannot capture localized deviations present in actual geometry. To improve result accuracy, simulations were performed with two tip clearance sizes: 2.8 mm (theoretically calculated) and 4.0 mm.

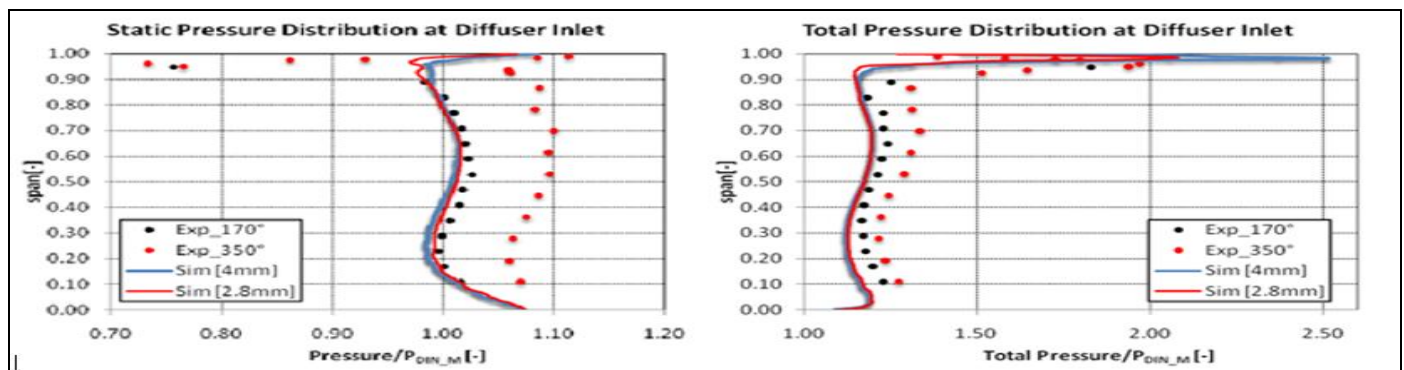


Fig 8 Relative Static (Left) and Total Pressure (Right) Distribution Vs Span At Diffuser Inlet

Figure 8 shows calculated and measured relative static and total pressure distributions over the span at the diffuser inlet. Measurements were taken at 170° and 350° circumferential positions. A good agreement is observed at 170°, while deviations at 350° are attributed to flow non-uniformity caused by the asymmetrical exhaust hood

geometry. Static pressure is well-predicted up to 95% span. At the tip jet region, static pressure is overestimated, while the total pressure matches well, implying an underestimated dynamic component. The 4.0 mm tip clearance yields a higher total pressure peak in this region.

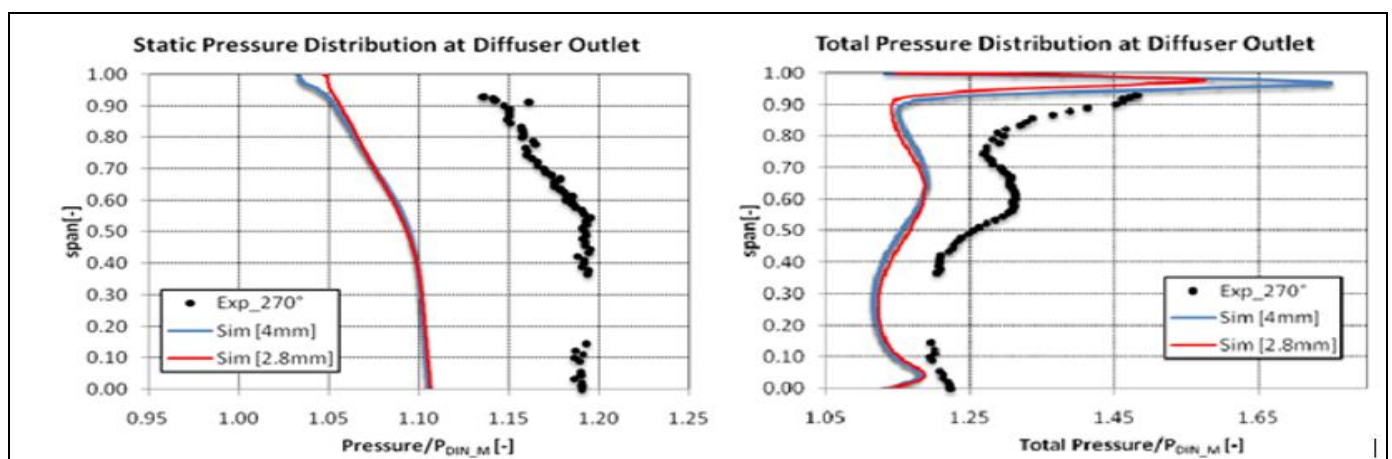


Fig 9 Relative Static (Left) and Total Pressure (Right) Distribution Vs Span At Diffuser Outlet

At the diffuser outlet (Figure 10), measurements from 12 o'clock are compared to CFD data from 6 o'clock, explaining an approximate 10% offset. Despite underestimation, the overall pressure trend and qualitative shape are captured well. Again, 4.0 mm clearance shows a greater total pressure at the tip region. Figure 10 presents the

static pressure distributions along the diffuser inner and outer shells. Inner shell predictions match well across circumferential positions, while outer shell deviations (up to 50% length) reflect secondary flow effects. Post 50%, both clearances yield good agreement, though the 4.0 mm clearance aligns slightly better.

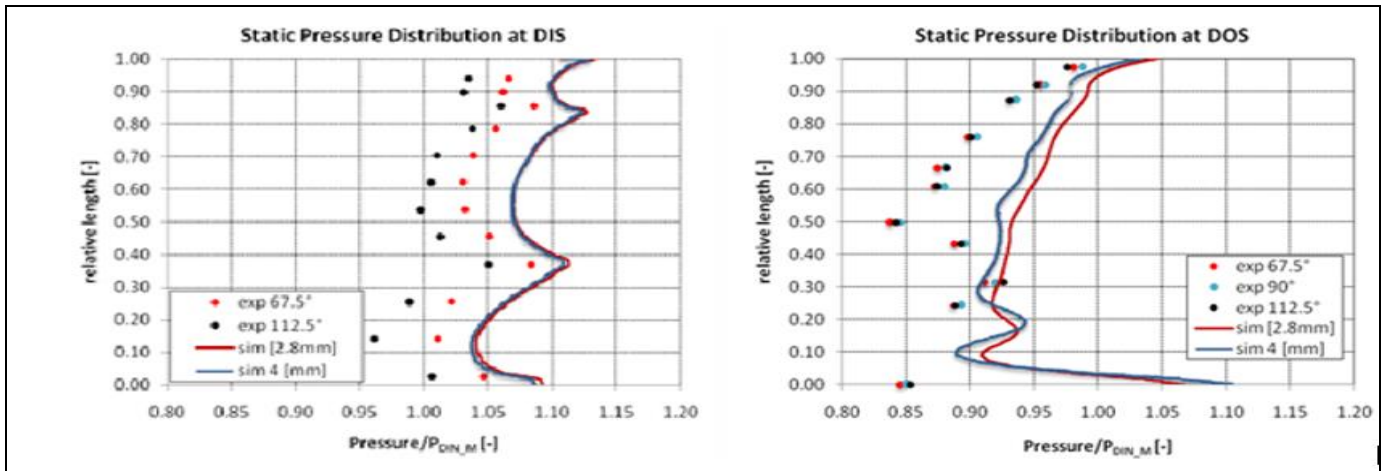


Fig 10 Static Pressure Distribution at Diffuser Inner Shell (DIS) and At Diffuser Outer Shell (DOS)

Figure 11 displays Mach number contours and velocity vectors, highlighting a thicker and more energetic tip jet with 4.0 mm clearance. Consequently, pressure recovery values in

Figure 12 are lower for 4.0 mm due to increased dissipation and higher total pressure at the diffuser inlet.

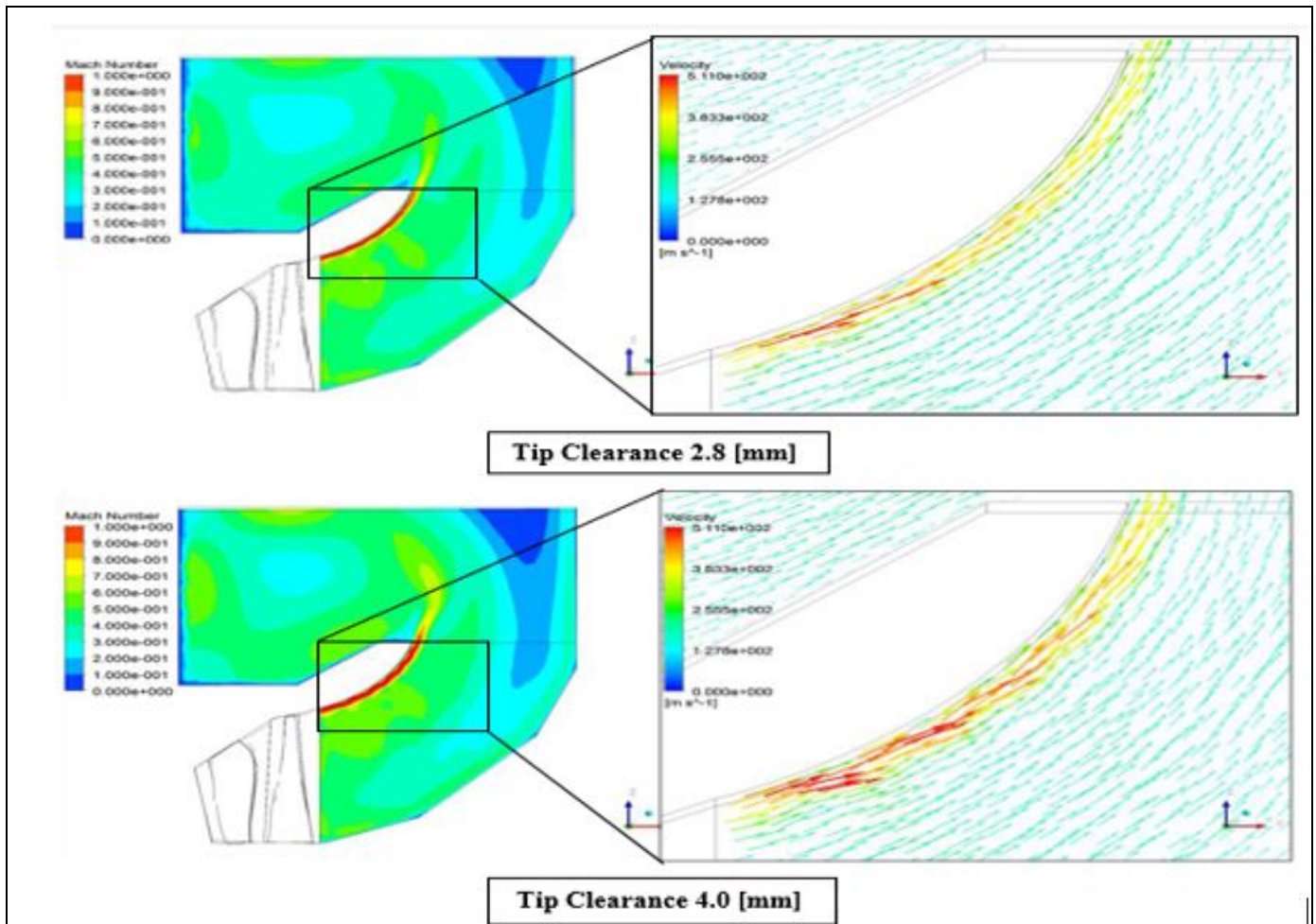


Fig 11 Mach number Contour Plots and Velocity Vectors at the Tip Jet Region of the Calculations with Distinct Tip Clearances

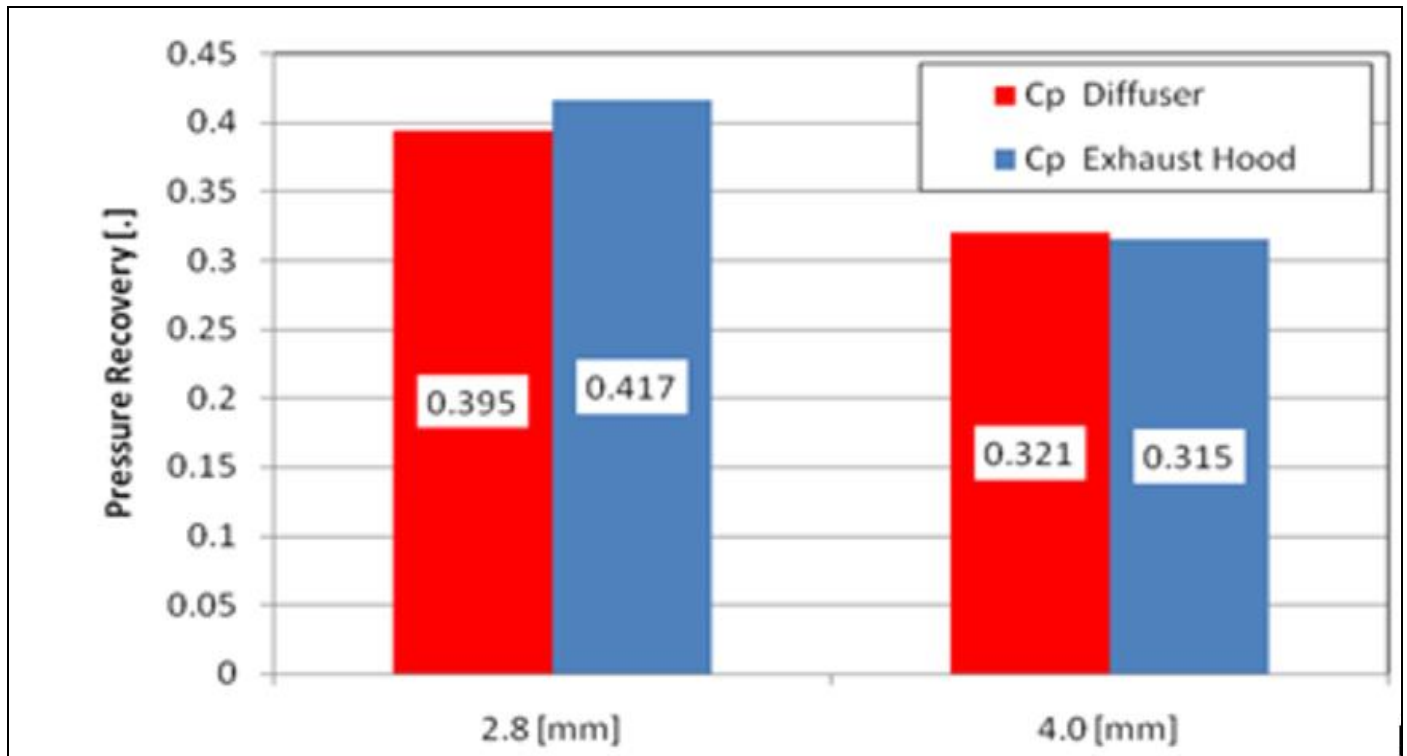


Fig 12 Diffuser and Exhaust Hood Pressure Recovery Values for the Calculations with Distinct Tip Clearances.

Given its improved agreement, the 4.0 mm tip clearance is adopted for further simulations.

• *Tip Clearance Analysis*

Mesh sensitivity analysis is carried out by systematically varying the mesh density to evaluate its impact on flow behavior. Separate studies were performed for the rotor and diffuser meshes.

• *Rotor Mesh Sensitivity*

Three different rotor meshes were used: Mesh I, Mesh II, and a finer Mesh III, with mesh densities of 62, 64, and 495 kNodes, respectively. The detailed mesh parameters are provided in Table 4. While Mesh I served as the baseline, Mesh II doubled the blade tip elements, and Mesh III was a refined version of Mesh I with a smaller wall-adjacent element size and increased resolution in the clearance region.

Table 4 Mesh data for different rotor meshes

	Mesh I	Mesh II	Mesh III
Mesh Density [kNodes]	62	64	495
Number of spanwise blade distribution elements	24	24	50
Size of the element next to the wall [mm]	1	1	0.5
Number of vertical elements in clearance region	5	5	10
Number of elements on blade tip	7	14	10
Y-plus average	84	88	38

Results showed only minor differences between Mesh I and Mesh II. However, Mesh III led to improved static pressure prediction at the tip jet region of the diffuser inlet, with reduced overestimation. The finer mesh also resulted in a smaller total pressure peak and increased dissipation, reflected in slightly lower pressure recovery values.

• *Diffuser Mesh Sensitivity*

Five different diffuser meshes were analyzed: a baseline mesh (107 kNodes), three directionally refined meshes (axial, circumferential, radial), and an overall refined mesh (829 kNodes). Details are provided in Table 5. For all these cases, the baseline rotor mesh was maintained.

Table 5 Mesh Data for Different Diffuser Meshes

	Mesh Density [kNodes]	Y-plus average
Basis Mesh (coarse)	107	14.14
Axially Refined	213	16.28
Circumferentially Refined	211	14.16
Radially Refined	213	1.65
Overall Refined	829	2.71

Pressure distributions at the diffuser inlet remained consistent across all meshes. At the diffuser outlet, however, noticeable differences emerged, particularly in the tip jet region. The overall refined mesh showed reduced pressure and total pressure at this region, indicating higher dissipation. Along the diffuser outer shell, pressure profiles varied up to 30% relative length, whereas the inner shell distributions were identical.

➤ *Diffuser In Stationary Reference Frame*

To examine the influence of reference frame and interface, four simulation approaches were evaluated as

summarized in Table 6. All used either the Frozen Rotor (FR) or Mixing Plane (MP) interface, with the diffuser domain in either rotating or stationary frame.

While diffuser inlet pressure results were similar across all approaches, significant deviations occurred at the outlet. The Mixing Plane with stationary diffuser (Approach IV) captured the tip jet more accurately and resulted in the highest pressure recovery values. In contrast, approaches using the Frozen Rotor interface failed to resolve the jet structure adequately, especially in Approach II and III.

Table 6 Distinct Approaches for the Calculations

Approach	Diffuser Mesh	Diffuser Frame of Reference	Interface between Rotor and Diffuser Domains
I	Baseline	Rotating	Frozen Rotor
II	Baseline	Stationary	Frozen Rotor
III	Overall fine	Stationary	Frozen Rotor
IV	Baseline	Stationary	Mixing Plane

➤ *Full Geometry Model Calculations*

• *Tip Clearance Analysis*

To determine a more representative rotor tip clearance for continued analysis, CFD simulations were conducted using two different tip clearance sizes: 2.8 mm, which is theoretically derived, and 4.0 mm, which reflects a more conservative design case. The goal was to identify the clearance value that yields results closer to experimental data while accurately resolving the tip jet flow characteristics,

which are critical for diffuser performance prediction. High-quality computational meshes were employed: multi-block structured meshes for the stator and rotor domains were generated using Ansys CFX Turbogrid, while the exhaust hood mesh, consisting of unstructured elements (tetrahedrons, wedges, and pyramids), and was created in Ansys Workbench. The mesh setup ensured sufficient resolution in key flow regions, particularly near walls and in the tip gap.

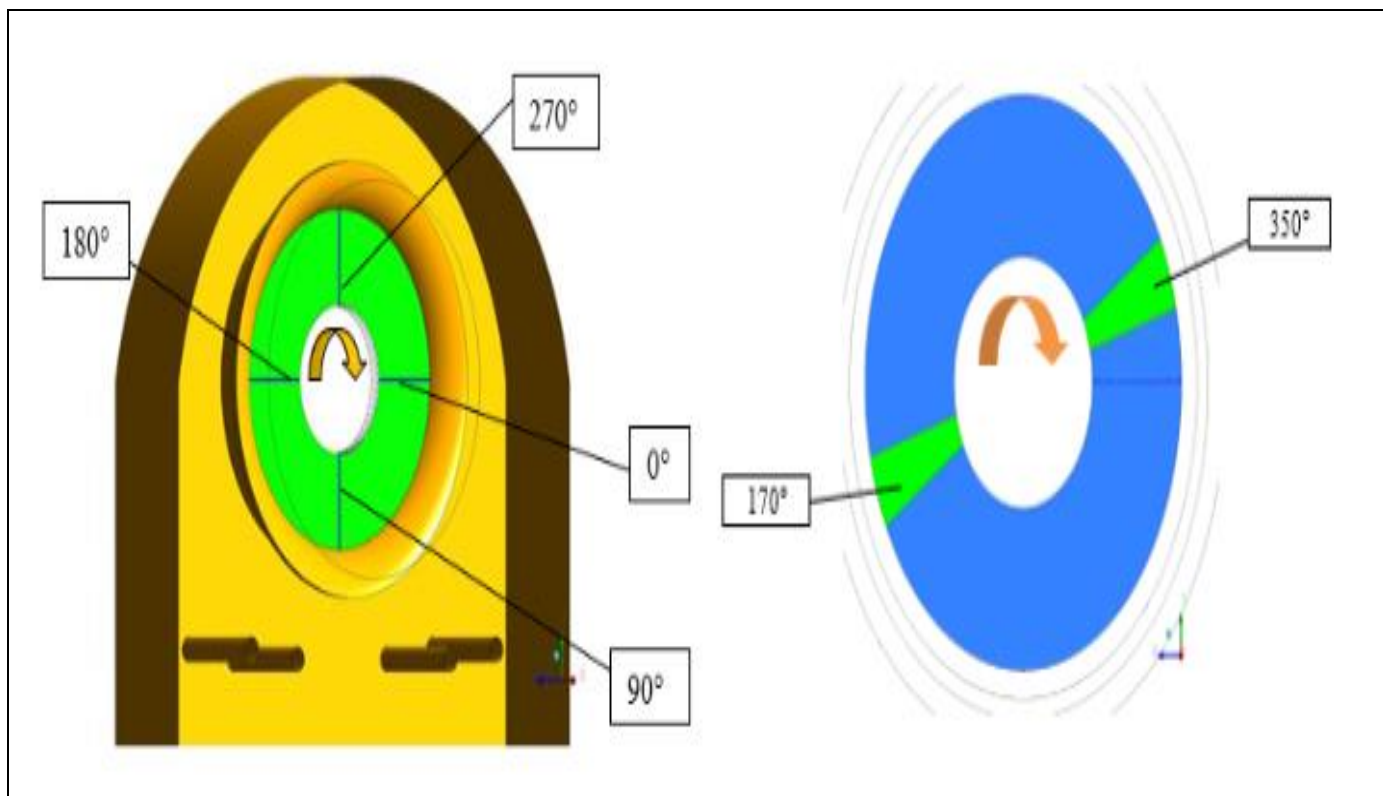


Fig 13 Evaluation Regions at the Diffuser

The circumferential measurement positions used for evaluation are shown in Figure 13. The calculated static and total pressure contour plots at the diffuser inlet for the 2.8 mm clearance case are presented in Figure 14, demonstrating a clear circumferential variation. Maximum and minimum pressures occur at 270° and 90°, respectively, consistent with expectations from the asymmetric exhaust hood geometry.

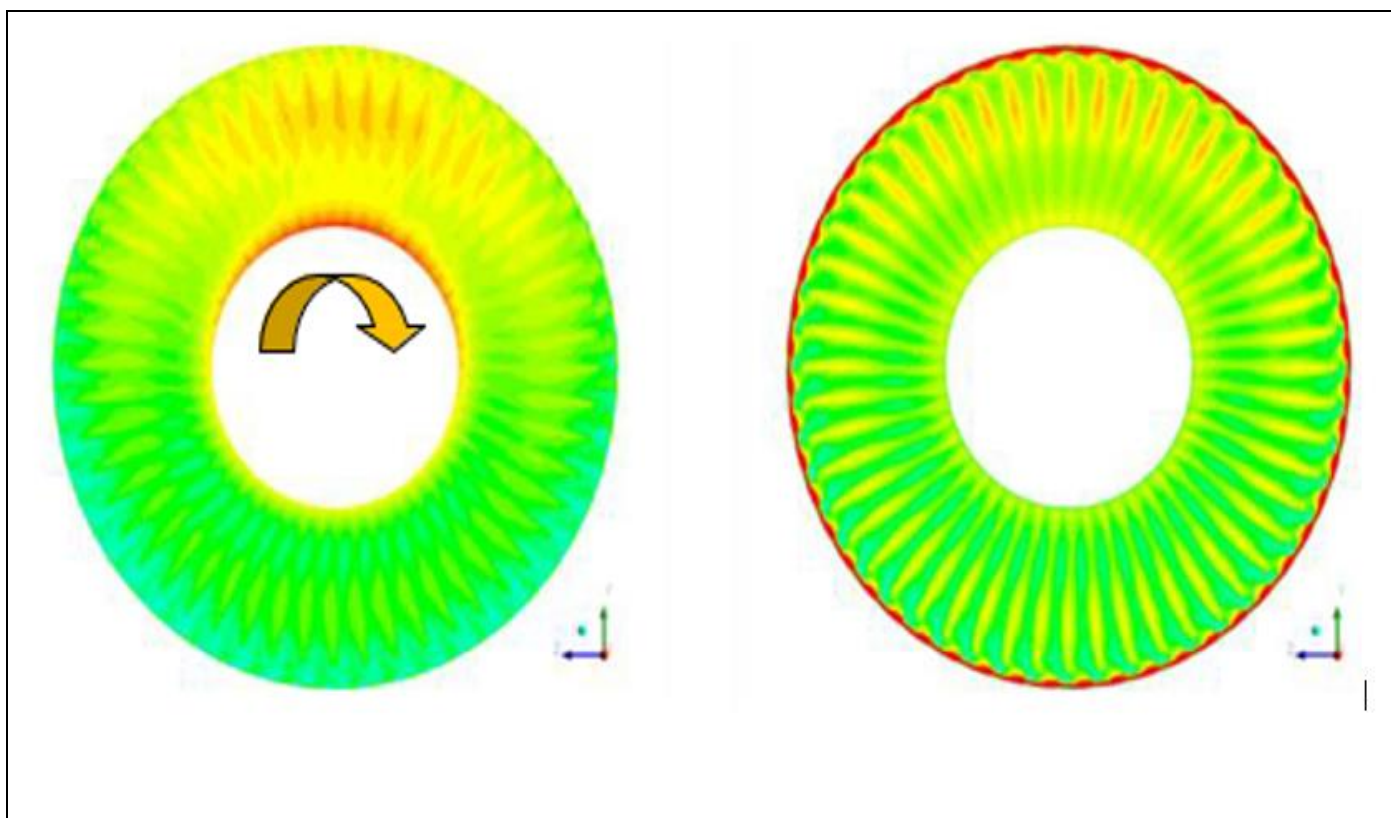


Fig 14 Static- And Total Pressure Contour Plots At the Diffuser Outlet (2.8 [Mm])

To visualize flow structures, streamlines were plotted (Figure 15), revealing swirling motion and vortex development within the exhaust hood. These spiraling steam paths confirm the presence of strong circumferential non-uniformity and highlight the importance of accurate modeling of the tip clearance effect.

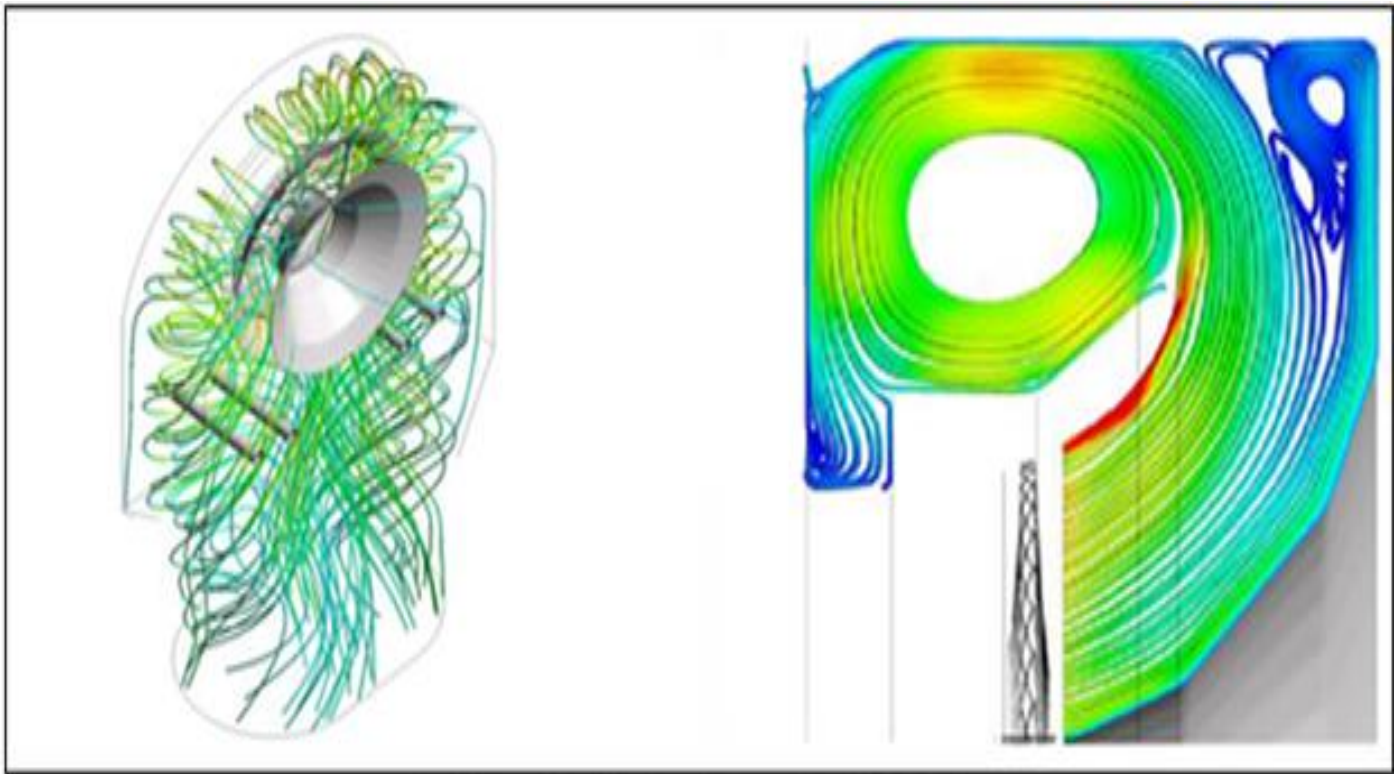


Fig 15 Flow Visualization via Streamlines (2.8 [Mm])

Measured and calculated spanwise static and total pressure distributions at the diffuser inlet were evaluated at two circumferential positions (170° and 350°). Both tip clearance cases exhibited good qualitative agreement with measurements; however, quantitative underestimation of pressure and total pressure was evident. The 2.8 mm clearance resulted in slightly smaller deviations from measurements, particularly at the 170° position, indicating a better match to real flow behavior.

At the diffuser outlet, the pressure profiles showed similar trends. The total pressure peak at the tip jet region was overestimated in the 4.0 mm case, indicating excessive kinetic energy retention. The 2.8 mm case showed a lower total pressure peak, closer to measured values, suggesting better resolution of dissipation effects in the tip jet region.

The static pressure distribution along the diffuser outer shell was also better represented by the 2.8 mm clearance, particularly in the second half of the diffuser length, where experimental data showed improved alignment. In contrast, pressure fluctuations in the first half of the diffuser, possibly caused by secondary flows, were not well captured in either case.

The key distinction between the two cases is the degree of dissipation at the tip jet region, as observed from the total pressure distributions at the diffuser outlet. The simulation with 4.0 mm tip clearance significantly overestimates the

total pressure maximum, indicating insufficient modeling of energy loss in that region. In contrast, the 2.8 mm clearance only slightly underestimates the peak, suggesting a more accurate representation of the flow behavior. Additionally, the 2.8 mm case demonstrates better agreement with measurements for the static pressure distribution along the diffuser outer shell, making it the preferred option for further numerical investigations.

➤ Tip Clearance Analysis

A detailed mesh sensitivity study was conducted using the full geometry exhaust hood model with the baseline 42 kNodes stator mesh and 62 kNodes rotor mesh at 2.8 mm tip clearance. The focus of this investigation was on variations in the exhaust hood mesh. Refinements were applied to different mesh regions: body refinement, inflation layer refinement, and diffuser surface refinement. In all cases, the total height of the inflation layer remained fixed.

At the diffuser inlet, the calculated static and total pressure distributions remained nearly identical across all mesh types, with minor quantitative underestimation relative to the measurements. At the diffuser outlet, all meshes showed similar pressure profiles up to 80% span. Beyond that, diffuser surface refinements introduced deviations, with stronger negative static pressure gradients and increased total pressure peaks, especially in the high-density mesh cases. This effect was most pronounced in the 8.29 MNodes mesh, indicating excessive non-uniformity and local pressure

distortions. Additional flow deviations were confirmed by comparing meridional Mach number contours and velocity vector plots, which showed that finer diffuser meshes generated wavier, non-uniform flow along the diffuser outer shell, particularly in the tip jet region. Such flow behavior was not observed with the coarser baseline mesh. Attempts to mitigate these deviations through domain segmentation and frozen rotor interface averaging were unsuccessful. Instead, the implementation of multiple stage interfaces between rotor and diffuser domains, each matching a single passage, produced more consistent and accurate flow behavior. The tip jet was resolved uniformly along the outer shell, and results became largely mesh-insensitive. Pressure and total pressure distributions at the diffuser outlet showed improved agreement with measurements when using this interface strategy. The pressure recovery values, especially $c_{p_diffuser}$, were also more accurate with the multiple mixing plane interface approach.

In conclusion, while finer meshes improve local flow resolution, they can introduce unwanted non-uniformities under frozen rotor assumptions. The multiple mixing plane approach proves more robust and reliable, delivering better accuracy and mesh independence under design load conditions.

➤ *Modifications*

The calculations presented so far demonstrate good qualitative agreement with experimental measurements, although quantitative deviations in static and total pressure distributions at the diffuser inlet and outlet persist. One major contributing factor is the assumption of ideal gas properties in the simulations, whereas the real turbine model involves wet steam. To address this, further calculations were performed using real gas properties, omitting condensation effects. Additionally, the ideal gas properties were adapted based on real gas behavior. All simulations in this section were conducted using multiple mixing plane interfaces between the rotor and exhaust hood domains. Despite these changes, the differences in pressure distributions between ideal, real, and adapted ideal gases were minor. However, the static pressure profile along the diffuser outer shell showed slightly better agreement with measurements when using real gas. In parallel, the total pressure at the stator inlet was increased by 5% to reflect measurement-based inflow boundary conditions more accurately. This adjustment improved the correlation of total pressure at the diffuser inlet but slightly worsened the static pressure agreement. At the diffuser outlet, both static and total pressure distributions improved quantitatively.

Another factor considered was the simplified geometry of the exhaust hood used in prior simulations. A more complex geometry, including carriers and probe structures, was introduced to better represent the experimental setup. This enhancement, however, did not significantly affect the pressure profiles at the diffuser inlet or along the diffuser inner shell. A notable zigzag pattern appeared along the diffuser outer shell pressure distribution, indicating stronger flow disturbances introduced by the enhanced geometry.

Lastly, simulations with enhanced geometry produced higher-than-expected exhaust hood pressure recovery values, contradicting assumptions about added geometric losses. This inconsistency suggests the need for further investigation into mesh sensitivity and convergence behavior with the enhanced exhaust hood model.

• *Off Design Operating Modes*

While previous calculations were conducted under design operating conditions, a comprehensive validation of the applied computational method requires simulations under off-design conditions as well. Steam turbines can be operated in different modes by either varying the condenser pressure or the mass flow rate. These variations correspond to part-load and overload operating modes, depending on the cooling water temperature and the corresponding adjustments to pressure or flow rate.

In this study, off-design simulations were performed by varying the mass flow rate while keeping the condenser pressure constant. This was achieved by adjusting total pressure and temperature at the stator inlet boundary. For part-load conditions, these parameters were decreased, and for overload, they were increased. Simulations were conducted using both frozen rotor and multiple mixing plane interfaces between rotor and exhaust hood domains. Mesh densities of 1.74 and 1.92 million nodes were used for the respective interface types. Results at the diffuser inlet show that, across all operating conditions, the calculated static and total pressure distributions qualitatively agree with measurements, though calculated values generally underestimate actual values. At the diffuser outlet, the agreement remains strong for design and part-load modes, regardless of interface method. However, under overload, the frozen rotor interface results in incorrect modeling of the tip jet region, significantly underestimating dissipation near the shroud. In contrast, the multiple mixing plane interface accurately resolves uniform tip jet flow. The static pressure distribution along the diffuser inner shell shows increasing pressure peaks at kink positions as mass flow rate increases. Along the outer shell, discrepancies between the two interface methods grow with higher mass flow rates, with the frozen rotor interface yielding less accurate predictions. Dynamic pressure fractions and circumferential variations are also affected. For design and part-load modes, both interface methods underestimate dynamic pressure, with the largest deviation at 170° under design conditions. Under overload, dynamic pressures are overestimated, particularly with the frozen rotor interface. Across all modes, frozen rotor calculations consistently yield higher dynamic pressure fractions than those from the multiple mixing plane approach.

Pressure recovery values are also underestimated in all scenarios. The multiple mixing plane method yields slightly higher recovery values and better consistency with trends in mass flow rate. This method proves more reliable in modeling pressure recovery and tip jet flow, especially under overload conditions. Therefore, the multiple mixing plane approach is more suitable for simulations across various operating modes.

- *Single Stage Exhaust Hood Model Calculations*

In addition to the validation calculations performed with the turbine model, further numerical investigations were carried out using the Siemens Single Stage Exhaust unit, as illustrated in Figure 16. This model comprises a single-blade stator domain, a full-blade rotor domain, and an exhaust hood domain. Simulations were executed using both frozen

rotor and multiple mixing plane interfaces between rotor and exhaust domains. The stator and rotor domains are coupled via a mixing plane interface employing circumferential velocity averaging. The standard k-epsilon turbulence model with scalable wall functions and ideal gas properties were applied for all simulations.

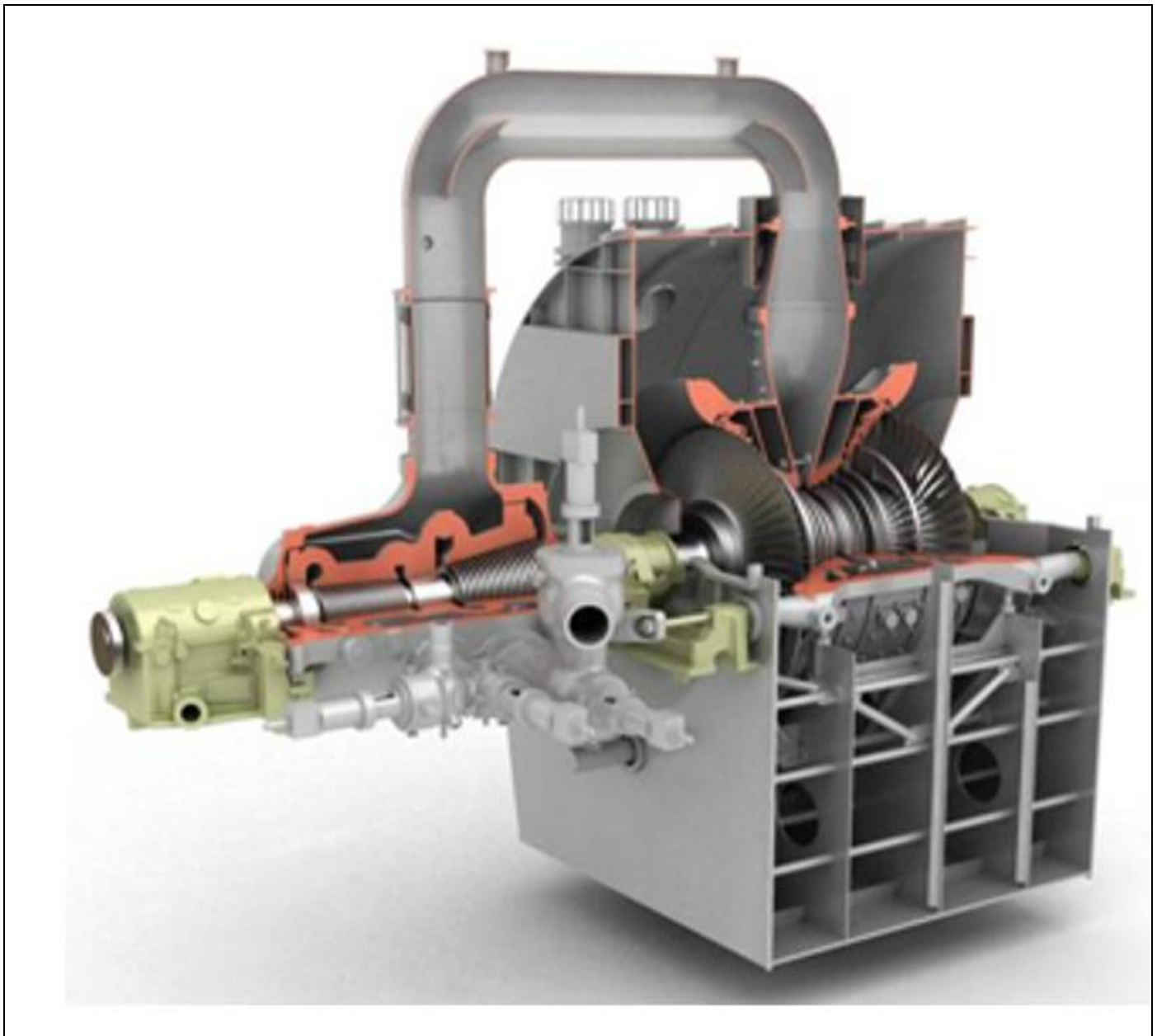


Fig 16 "Siemens" Single Stage Exhaust Steam Turbine

The exhaust hood geometry used in the calculations is shown in Figure 17. As with the model turbine, structured meshes were generated for the stator and rotor domains using Ansys CFX Turbogrid, while the exhaust hood was meshed with unstructured tetrahedral, wedge, and pyramid elements in Ansys Workbench. The stator and rotor meshes contained 44,000 and 3.35 million nodes, respectively, while the exhaust hood mesh had a density of 11.42 million nodes.

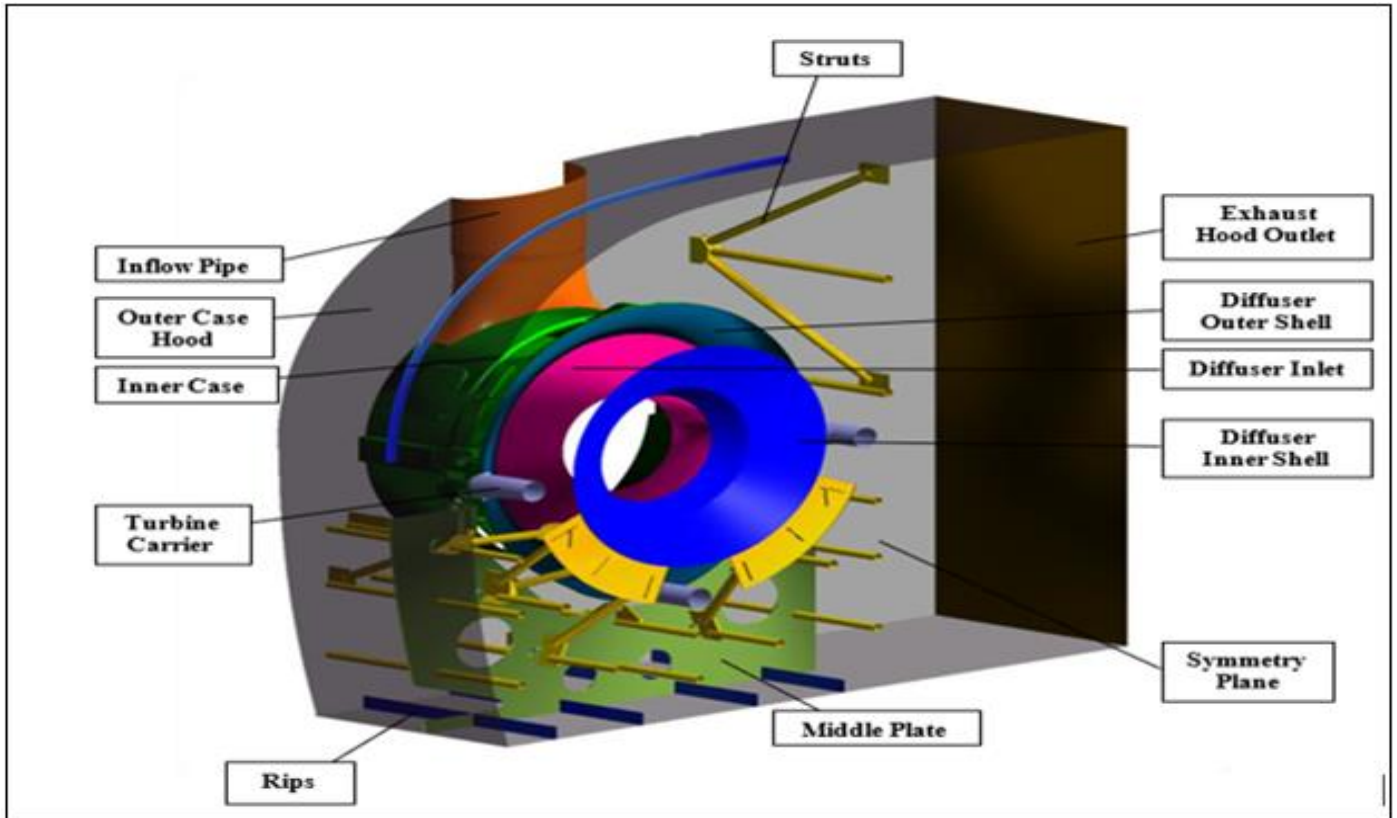


Fig 17 Single Side Exhaust Hood

Simulations were run for six different operational conditions by varying condenser pressure, allowing the analysis of part load, design load, and overload cases. Figure 19 compares the axial Mach numbers calculated with the two interface approaches. Under part load ($P_{cond} = 8000$ Pa,

9500 Pa), the Mach numbers from both approaches are nearly identical. However, under design and overload conditions (e.g., $P_{cond} = 4000$ Pa), noticeable differences emerge, with the multiple mixing plane approach producing higher Mach numbers.

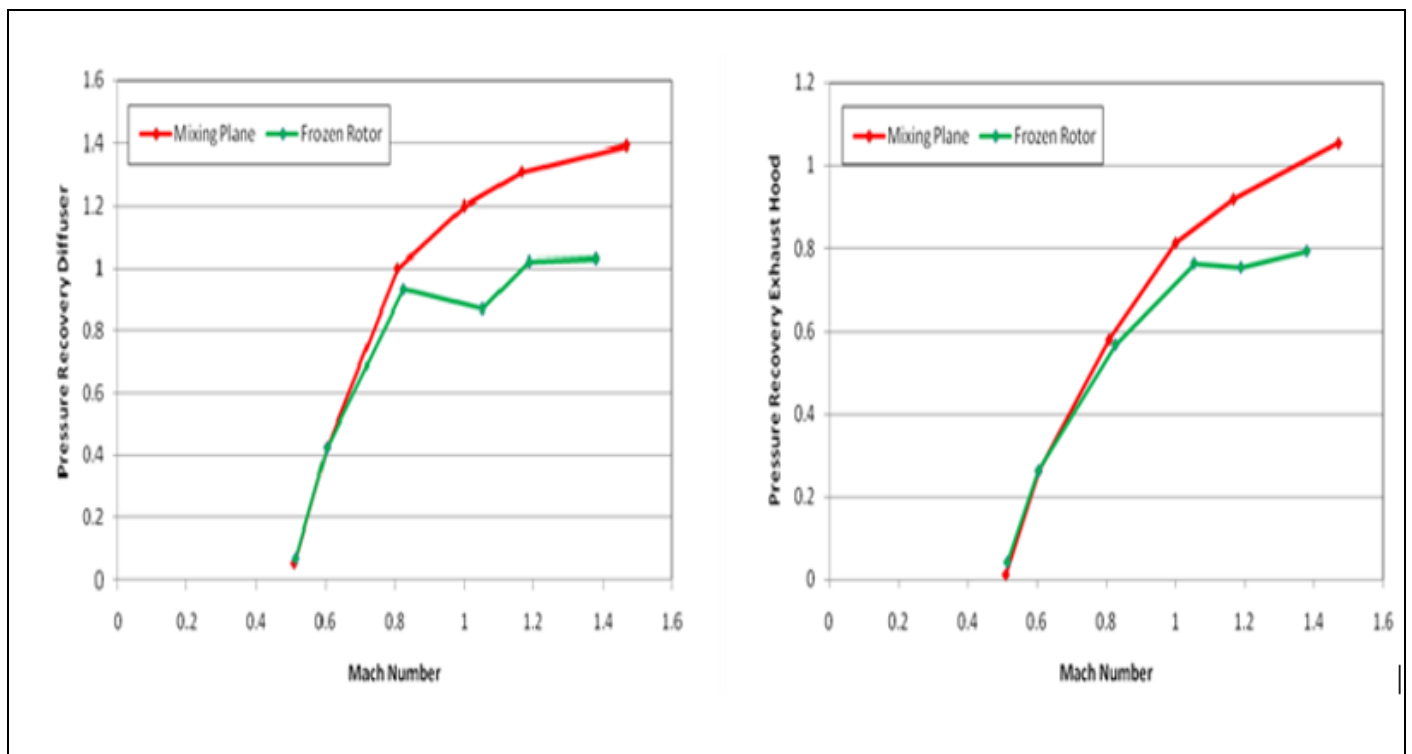


Fig 18 Diffuser (Right) and Exhaust Hood (Left) Pressure Recovery Values Plotted Against Mach Numbers

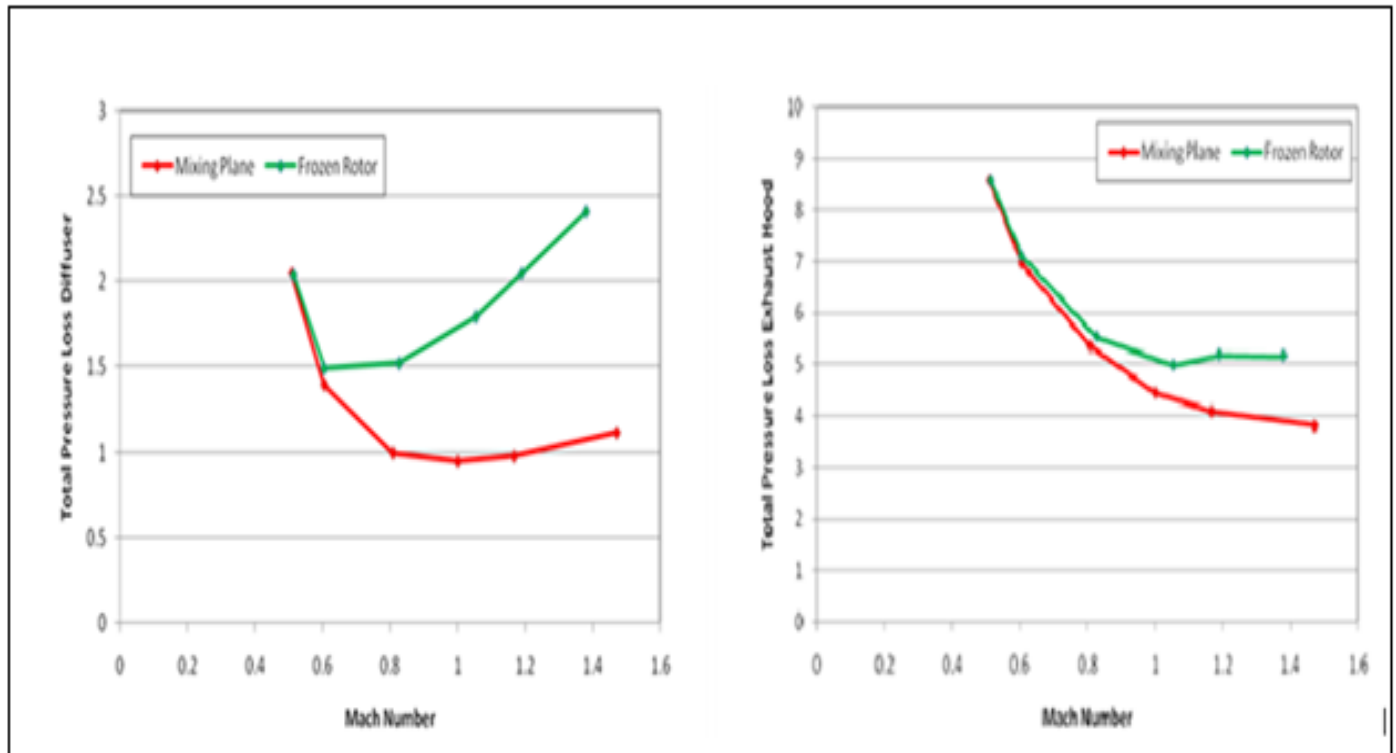


Fig 19 Diffuser (Right) and Exhaust Hood (Left) Total Pressure Losses Plotted Against Mach Numbers

The circumferential static and total pressure variations at the diffuser inlet were also analyzed, with a focus on 90% span. The largest variations were found at $P_{cond} = 4500$ Pa, with decreasing values at higher condenser pressures, attributed to increased circumferential flow uniformity. In general, the frozen rotor approach resulted in slightly smaller circumferential variations.

At the diffuser outlet, significant differences were observed between the two methods under overload conditions, particularly near the shroud tip jet region, where the frozen rotor method underestimated the total pressure due to non-uniform jet development. This discrepancy diminishes at higher condenser pressures and disappears entirely under part load. Interestingly, under extreme part load ($P_{cond} = 9500$ Pa), the frozen rotor approach yields a higher total pressure peak at the tip jet, reversing the typical trend seen under overload.

Finally, Figure 20 illustrates the total pressure losses versus axial Mach number. Above $Ma = 0.60$, losses are consistently higher when using the frozen rotor interface. Notably, the total pressure loss in the diffuser increases sharply for the frozen rotor approach, while only slight gradients are observed with the multiple mixing plane interface.

Overall, the differences between the two interface methods become most pronounced under design and overload operating conditions.

• *Geometry Modifications*

To improve the efficiency of the steam turbine, a series of geometrical modifications were applied to the exhaust hood. All simulations were carried out at design load operating conditions with a condenser pressure of 6000 Pa, using multiple mixing plane interfaces between rotor and diffuser domains. The geometries considered in this study are listed as follows:

- ✓ Original exhaust hood
- ✓ Exhaust hood with middle plate containing bigger holes
- ✓ Exhaust hood with middle plate without holes
- ✓ Exhaust hood without 5 bottom struts
- ✓ Exhaust hood without middle plate
- ✓ Exhaust hood without upper struts
- ✓ Exhaust hood without bottom struts
- ✓ Exhaust hood without middle plate and bottom struts

The flow induced by these modifications becomes increasingly turbulent, which affects simulation convergence.

First, circumferential pressure variations at 90% span were investigated. The normalized variations ($P_{var_90\%}$) reveal that the geometry with no holes in the middle plate (3) produces the largest circumferential pressure variation, which is consistent with the observation that blocked flow paths increase pressure gradients. Except for the model without upper struts (6), all other modifications result in smaller pressure variations compared to the original geometry.

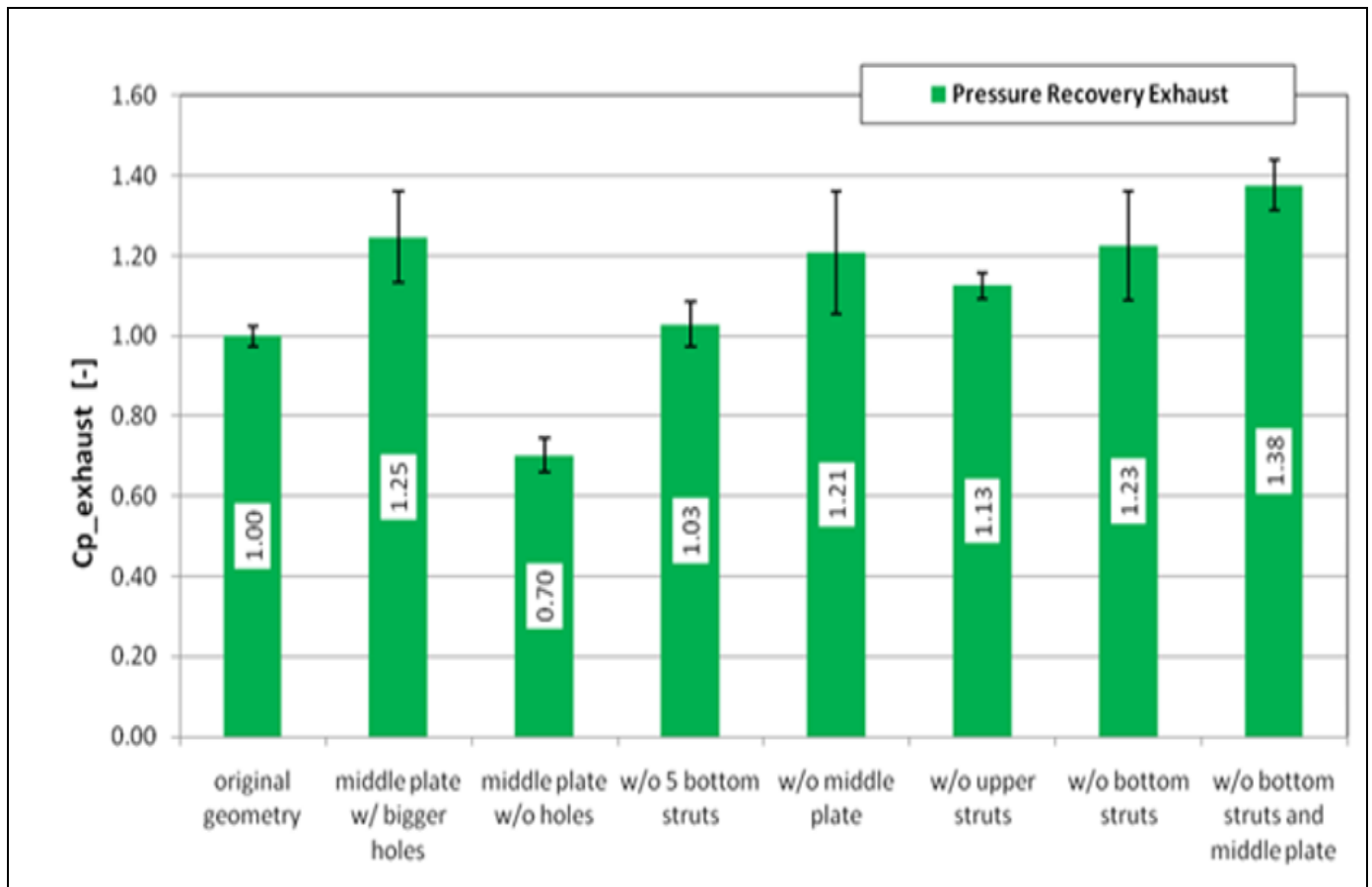


Fig 20 Pressure Recovery Values For Distinct Geometries

Figure 20 presents the exhaust hood pressure recovery factors ($cp_{exhaust}$) for each configuration. Values were normalized to the $cp_{exhaust}$ calculated for the original geometry. The highest pressure recovery is achieved with the geometry without the middle plate and bottom struts (8), while the lowest is observed with the geometry without holes in the middle plate (3). Notably, the middle plate with larger holes (2) yields a $cp_{exhaust}$ improvement of approximately 0.06, while geometry 8 achieves an increase of 0.09.

In conclusion, enlarging the holes in the middle plate offers a practical and effective geometrical modification for improving steam turbine exhaust performance.

IV. CONCLUSION

In the framework of this research, several numerical analyses using CFD software Ansys CFX were conducted, to validate and apply the Last Stage Modeling (LSM) method under various modeling assumptions and boundary conditions.

The first phase of the study focused on validating the LSM method by comparing numerical results with experimental data obtained from a model steam turbine exhaust setup. Two types of computational domains were used: the one-passage last stage exhaust model and the full geometry exhaust model. These investigations evaluated the influence of various factors, including rotor tip clearance, mesh density, interface type, working fluid properties, inlet

boundary conditions, exhaust hood geometry, and operating modes.

Regarding tip clearance, simulations were carried out for 2.8 mm and 4.0 mm configurations. The 4.0 mm clearance performed better in the one-passage model, while 2.8 mm clearance was preferred for the full geometry model, where it provided a more accurate tip jet and static pressure distribution. The larger clearance generally resulted in lower pressure recovery, largely due to higher total pressure at the diffuser inlet.

Mesh sensitivity analyses showed that in the one-passage model, using a finer diffuser mesh with a frozen rotor interface resulted in stronger and longer-lasting clearance vortices. In the full geometry model, using the frozen rotor interface with a fine exhaust mesh led to a non-uniform tip jet that weakened sharply, whereas the multiple mixing plane interface generated a stable and mesh-independent tip jet. The latter interface consistently yielded higher pressure recovery factors.

The analysis also explored the influence of material properties and inflow boundary conditions. Switching from ideal gas to real gas as a working fluid produced only a minor improvement in matching measured and calculated pressure profiles. Increasing the total pressure at the stator inlet and modifying the exhaust hood geometry had no significant effect. Surprisingly, the enhanced exhaust hood

geometry led to higher pressure recovery, contrary to the expected outcome due to increased loss sources.

The off-design condition analysis further validated the LSM method. While both frozen rotor and mixing plane interfaces showed good agreement at design and part load, the frozen rotor interface failed under overload conditions, where it could not correctly model the tip jet. The multiple mixing plane interface, however, retained accuracy under all operational loads.

In the second phase, the LSM method was applied to the Siemens Single Stage Exhaust model, tested under various operating modes. Once again, the mixing plane approach demonstrated superior robustness and accuracy across a wide Mach number range, particularly under overload conditions.

Finally, numerical simulations were conducted with modified exhaust geometries. Among the variants tested, enlarging the holes in the middle plate resulted in a significant increase in $cp_{\text{exhaust_hood}}$. Given its effectiveness and simple implementation, this modification is recommended as a viable measure to improve steam turbine performance.

Overall, the study confirms that the multiple mixing plane interface is the most reliable and versatile option for accurate steam turbine flow modeling using the LSM method.

REFERENCES

- [1]. Polklas, Thomas. Essen : s.n., May 2004, Universität Duisburg Essen, Dissertation. "Entwicklung eines numerischen Verfahrens zur strömungsmechanischen Auslegung des Abströmgehäuses einer Niederdruck-Dampfturbine."
- [2]. Hurtado, Fernando Sandro Velasco, Maliska, Clovis Raimundo und Cordazzo, Jonas. 2005. CILAMCE 2005 "An Element-based Finite Volume Formulation for Reservoir Simulation. "
- [3]. Moore, M.J. "Aerothermodynamics of Low Pressure Steam Turbines and Condensers."
- [4]. Otterfing 1998 Siemens-intern "Technical Report AEAT/TR-98-11 Berechnung des dreidimensionalen Strömungsfeldes in Modellturbinenstufen mit CFX-TASCflow."
- [5]. Denton, J.D. "The calculation of three-dimensional viscous flow through multistage turbomachines." 1992, Transactions of the ASME, Journal of turbomachinery, Bd. 114, S. 18-26.
- [6]. Denton, J.D. "Computational Methods for Turbomachinery Flow." 1986. ASME Course Fluid Dynamics Turbomachinery, Lecture 9, P. 13-1 to 13-41.
- [7]. Denton, J.D. "Loss Mechanismus in Turbomachines. " 1993, ASME Journal of Turbomachinery, Bd. 115, S. 621-656.

- [8]. Gloss, Dr. D. "Replacing the "Coupling Tool" by Last Stage Modeling for calculating exhaust steam flow". Siemens-Intern.
- [9]. ITSM Presentation "Cp-Wert Diffusor.ppt".